Origin of graphitic bands in graphite intercalation compounds

R. S. Markiewicz
Department of Physics, Northeastern University, Boston, Massachusetts 02115
(Received 1 June 1987; revised manuscript received 25 September 1987)

The stage dependence of the electronic bands near the Fermi surface of graphite intercalation compounds is discussed. Special attention is paid to the interlayer coupling and to the origins of the small, graphitelike bands. Applications are made to the stage dependence of the anisotropy and temperature dependence of the conductivity. Numerous formulas are included to allow ease of comparison to experiment.

I. INTRODUCTION

There has been considerable interest in the past few years in the experimental realization of "two-dimensional metals."[1] While a number of criteria for two dimensionality exist, the following, high-magnetic-field criterion is of particular significance: A metal can be considered to be two dimensional in a strong magnetic field if successive Landau levels do not overlap in energy. This has been shown[2] to be a necessary condition for the observation of the quantum Hall effect[3] (QHE).

Much interest has been generated by the QHE, and most studies of the two-dimensional electron gas (2D EG) have been carried out in the Si inversion layers and GaAs heterojunctions where this effect was first discovered. Nevertheless, these materials have certain disadvantages: the low carrier density and small sample volumes make it difficult to measure bulk properties (heat capacities, magnetization).[4] Naturally layered bulk materials offer an alternative means of studying the 2D EG, and recent studies on one family, the Bechgaard salts, suggest that there is interesting new physics associated with the dense 2D EG.[5] An outstanding problem in analyzing layered compounds is just how two dimensional they are: For instance, do they satisfy the above-mentioned 2D criterion?

Graphite intercalation compounds[6] (GIC's) offer an important test case. By varying the intercalant species, the conductivity anisotropy can be varied over five orders of magnitude, from nearly isotropic to the most anisotropic layered compounds known. At the same time, the in-plane band structure can be well represented by the same tight-binding model which works in pure graphite. Hence it seems auspicious to try to incorporate coupling of the graphite bands *across* the intercalant—to directly estimate the dispersion of the GIC energy bands in the third dimension (along the c axis), to determine just how two dimensional these materials really are. Recently, this band dispersion and the resulting conductivity anisotropy were calculated for compounds of stage 1 (Ref. 7) and stage 2 (Ref. 8) (the stage number is the number of graphite layers separating successive intercalant layers). The overall comparison with experiment was quite encouraging, and more recent results have tended to support the general picture. This paper extends these calculations to higher stages, which are important in understanding the genesis of the semimetallic graphitelike bands associated with the graphite layers which are not immediately adjacent to an intercalant layer (*interior* layers, as opposed to *boundary* layers). The results are in qualitative agreement with experiments on the stage dependence of the c-axis anisotropy. Simplified expressions for the results are included, in the hopes that these will be useful in more quantitative comparisons of experiment and theory.

The paper is organized as follows. Section II recapitulates the earlier calculation, and cites more recent evidence in support of the result. Section III generalizes the tight-binding equations to higher stage, and reduces them to a form suitable for numerical calculations. Results of these calculations are presented in Sec. IV. To clarify the interpretation of these results, approximate calculations are also presented, which are simpler to deal with and yet preserve the characteristic features of the general results. While general results are presented for the boundary layers, the interior layers are only solved for stages 3–6. In Sec. V, these simplified bands are applied to a model calculation of the conductivity, and explicit predictions of the stage dependence (and temperature dependence) of the conductivity are made and compared with experiment. Section VI provides a summary.

II. OUTLINE OF METHOD AND RESULTS FOR STAGE 1

The three-dimensional π bands of pure graphite, in the neighborhood of the Fermi energy, were originally calculated in a tight-binding model by Slonczewski, Weiss, and McClure[9] (SWM). The energy determinant can be recast in a layer-by-layer form (each pair of wave functions associated with a particular carbon layer). If overlap of wave functions across the intercalant layer is entirely neglected, the resulting determinant couples carbon layers only between a particular pair of intercalant layers. This *single-sandwich* SWM (SSWM) approximation gives a good account of the in-plane band structure of acceptor GIC's, allowing predictions of optical properties[10] and Fermi surface areas.[11] However, since intersandwich overlap is ignored, the Fermi surfaces are two-dimensional (no energy dispersion along the c axis) and the c-axis resistivity is infinite.

The SSWM was originally introduced by Blinowski

et al.[10] in a restricted form, ignoring all the SWM parameters except γ_0,γ_1, and later generalized to include all the SWM parameters (but no screening) by Holzwarth.[12] A model including band overlap was introduced by Leung and Dresselhaus and Shayegan *et al.*[13] to describe the alkali metal GIC's. This overlap produces a finite c-axis dispersion and conductivity, but the overlap parameters were assumed to be unchanged from the graphite values. The variation of overlap energy with layer separation was studied in Ref. 7. For overlap parameter B, the c-axis conductivity is proportional to B^2 and by comparing the conductivity anisotropy of a number of intercalation compounds, it was found that

$$B \propto \exp(-I_c/I_{c0}) , \tag{1}$$

where I_c is the carbon-carbon separation distance across the intercalant layer and $I_{c0}\cong 0.71$ Å. This single Eq. (1) is consistent with virtually all the data for stage-1 compounds. Since this model was published, a number of results have appeared which are in agreement with the model.

(1) B has been directly measured from Fermi surface studies in $SbCl_5$ (Ref. 14) and Br_2 (Ref. 8) GIC. In both cases, B agreed with the model prediction within a factor of 2. In the latter case, detailed susceptibility line-shape analysis confirmed that the 2D EG was indeed in the 2D limit.

(2) A rule of thumb in GIC studies had been that donor intercalation reduces the conductivity anisotropy of pure graphite, while acceptor intercalation enhances it. According to the new model,[7] this is just a coincidence of the fact that the donors studied were alkali metals with small I_c values, while the acceptors had large I_c's. New studies of donor compounds with large I_c values[15] find a large anisotropy, comparable to that of acceptor compounds.

(3) If the only purpose of the intercalant is to modulate the overlap by varying I_c, then it should be possible to produce the same changes through totally different means—in particular, by varying the carbon-carbon separation via hydrostatic or uniaxial pressure. Indeed, studies on pure (unintercalated) graphite find that the overlap energy parameters $(\gamma_1,\gamma_2,\gamma_5)$ obey Eq. (1) with essentially the *same* value of I_{c0} ($I_{c0}\cong 0.5$–1.0 Å).[16]

III. BAND-STRUCTURE CALCULATIONS

The starting point of the calculation is the single sandwich SWM model. Since there are two atoms per unit cell per layer, the energy determinant for stage n will be of order $2n\times 2n$. The determinant for stage 4 (with interlayer coupling included) is

$$\det\begin{vmatrix}
-E_b & -\Gamma_0^* & -\gamma_1 & \Gamma_4 & \gamma_5 & 0 & \Gamma_1 & 0 \\
-\Gamma_0 & -E_b & -\Gamma_4 & 0 & 0 & \gamma_2 & 0 & \Gamma_2 \\
-\gamma_1 & -\Gamma_4^* & -E_i & \Gamma_0 & -\gamma_1 & -\Gamma_4^* & \gamma_5 & 0 \\
\Gamma_4^* & 0 & \Gamma_0^* & -E_i & \Gamma_4^* & 0 & 0 & \gamma_2 \\
\gamma_5 & 0 & -\gamma_1 & \Gamma_4 & -E_i & -\Gamma_0^* & -\gamma_1 & \Gamma_4 \\
0 & \gamma_2 & -\Gamma_4 & 0 & -\Gamma_0 & -E_i & -\Gamma_4 & 0 \\
\Gamma_1^* & 0 & \gamma_5 & 0 & -\gamma_1 & -\Gamma_4^* & -E_b & \Gamma_0 \\
0 & \Gamma_2^* & 0 & \gamma_2 & \Gamma_4^* & 0 & \Gamma_0^* & -E_b
\end{vmatrix} = 0 . \tag{2}$$

From this the determinant for any other stage may be readily constructed by adding (or subtracting) rows and columns. In this equation, $\Gamma_0=\gamma_0\sigma e^{i\alpha}$ and $\Gamma_4=\gamma_4\sigma e^{i\alpha}$, where $\sigma=\sqrt{3}k_\rho a_0/2$; k_ρ is the in-plane wave number, $a_0=2.46$ Å, and α is the angle between k_ρ and a graphite (100) direction. The γ's are SWM energy overlaps, and are taken to have values[11,17] $\gamma_0=3$ eV, $\gamma_1=0.39$ eV, $\gamma_2=-0.02$ eV, $\gamma_4=0.18$ eV, and $\gamma_5=-0.006$ eV. The SWM parameters Δ and γ_3 have negligible effect on Fermi surface areas,[11] and have been neglected. Just as in pure graphite, the second layer parameters γ_2 and γ_5 are necessary to turn zero-gap semiconducting bands into small semimetallic pockets. The smaller parameter, γ_5, is not important, and will be set to zero in the approximate analyses. The parameter $\Gamma_1=Be^{i\phi}$, with $\phi=k_zI_c$, is the intersandwich overlap parameter. As discussed in Refs. 7 and 8, a number of different overlaps can occur, but the particular matrix elements chosen do not greatly influence the result. The form Γ_1 [its position in the determinant Eq. (2)] is the most commonly occurring, as well as the simplest to handle, and so will be used in most of this paper. However, in discussing interior layers, it will be convenient to introduce a second overlap parameter, $\Gamma_2=B_2e^{i\phi}$. Outside of Sec. IV D, this additional complication will be ignored, and Γ_2 set equal to zero.

The notation E_b,E_i for the diagonal matrix elements must be carefully explained. The zero of energy is defined to be at the center of the interior graphite π bands, near the **k** point in the graphite Brillouin zone (the point at which, in strictly two-dimensional bands, the valence and conduction bands just touch). Then $E_i=E$, $E_b=E+\mu$, where μ is a band offset due to c-axis screening[10,18]—because the intercalant layer is ionized, carriers in the graphite layers are preferentially attracted to the layer nearest the intercalants. For higher-stage compounds, there can be inequivalent interior layers, for

which the additional offset parameter $\bar{E}_i$ is introduced below, although in general it will be assumed that $E_i=\bar{E}_i$ (Raman spectra show that there is only a single interior layer peak whereas the boundary layer peak is well separated, due to extra charge transfer). The meaning of E_b, E_i is most easily understood in the limit $\gamma_2,\gamma_5=0$. In this case the boundary and interior layers are decoupled, and independent carrier densities can be defined, with $n_{b(i)} \propto E_{b(i)F}$, where n_b is the carrier density in the boundary layer, E_{b_F} is the value of E_b at the Fermi energy, $E=E_F$. The proportionality of $n_{b(i)}$ to $E_{b(i)}$ will also approximately hold in real intercalation compounds, since γ_2 and γ_5 are so small. Thus, for instance, if $E_{iF}=0$, the interior layers are zero-gap semiconductors.

The case $E_{iF}=0$ is of special importance, since it corresponds to pure graphite. The band overlap is due solely to the γ_2,γ_5 parameters, and the net carrier concentration (density of holes minus density of electrons) is ideally zero. A simple model[19] of high-stage GIC's assumes that, at least for stages greater than 4, the interior layers are essentially graphitic, $n_i=0$. Most of the applications of the present manuscript are restricted to a generalization of the above model, assuming $E_{iF}=\bar{E}_{iF}=0$. However, energy dispersion formulas are provided for arbitrary values of $E_i,\bar{E}_i$, and so could be used for a different choice of Fermi level. de Haas–van Alphen results on acceptor GIC's suggest that the approximation $E_{iF}=0$ is poorest for stages 3 and 4, where $\sim 15\%$ of the carriers are in the interior layers,[20] but should be quite good by stage 7. Taking $E_{iF}=0$ represents a natural generalization of Ref. 19. In that reference, the interior layers were assumed to have the full, three-dimensional graphite energy bands. However, in a GIC, the c-axis dispersion is considerably weaker, and an important result of this paper is to show how the c-axis dispersion of the interior layers develops as the stage number is increased—that is, how a GIC evolves into graphite.

Experimentally, it is found[11,20] that the net charge transferred to the graphite layers depends strongly on the intercalant, but only weakly on stage. Because of the proportionality of $n_{b(i)}$ to $E_{b(i)}$, the stage dependence of the total density $n_0=2n_b+(n-2)n_i$ (for $n\geq 2$) may be expressed directly in terms of energies, defining $E_{F0}=E_{bF}(n_0/n_b)$. The present model assumes a stage-independent density, fixed by imposing

$$E_{F0}=\begin{cases}2E_{bF}+(n-2)E_{iF}, & n\geq 2\\ E_{bF}, & n=1\ ,\end{cases} \tag{3}$$

where n is the stage number and E_{F0} varies with the intercalant. (This equation is only approximately true when $\gamma_2\neq 0$.)

Equation (2) (or its generalization for stage n) may be simplified. By multiplying all of the even wave functions by $e^{i\alpha}$ or $e^{-i\alpha}$ and by judicious sign changes, all of the matrix elements involving Γ_0,Γ_4 can be made real and positive. In this case, the determinant of Eq. (2) is purely real, except for the Γ_1 term (this means the bands have cylindrical symmetry in the conducting plane which would not be true if $\gamma_3\neq 0$). If Γ_1 were real, the determinant would be completely symmetrical upon interchanging the first and $(n-1)$st elements, second, and nth, etc. This reflects the layer symmetry of the sandwich. By taking symmetric and antisymmetric combinations of the carriers in the two boundary layers, and simultaneously, of carriers in the corresponding interior layers, the determinant equation can be separated into the product of two determinants, one involving symmetric states, one antisymmetric. Then a $2n\times 2n$ determinant equation is simplified to two lower-order equations. If n is even, the lower-order determinants are both $n\times n$; for odd n, one (the symmetric) is $(n+1)\times(n+1)$; the antisymmetric is $(n-1)\times(n-1)$ with the innermost layer uncoupled.

Since Γ_1 is complex, the actual procedure is slightly more complicated. If Γ_1 is written $\Gamma_{1c}+i\Gamma_{1s}$, where Γ_{1c} and Γ_{1s} are real, then if $\Gamma_{1s}=0$, the separation $D=D_sD_a$ would hold, where D is the determinant of Eq. (2) and D_s and D_a are the symmetric and antisymmetric subdeterminants introduced above, now including Γ_{1c}. For $\Gamma_{1s}\neq 0$, it can be shown that $D=D_sD_a-\Gamma_{1s}^2\hat{D}_s\hat{D}_a$, where $\hat{D}_s$ ($\hat{D}_a$) is the matrix derived from D_s (D_a) by deleting the row and column which involve Γ_{1c}. When Γ_1 is small, the additional term may be neglected. The determinants are now in a suitable form for numerical calculations. The resulting energy dispersion (k_ρ versus k_z for fixed E_{bF},E_{iF}) will be discussed in the following section, where simplified approximations to the dispersion are derived.

IV. RESULTS AND APPROXIMATIONS

A. In-plane structure: Cylinders versus pockets

From the SSWM model, it is known that there are approximately n Fermi surface sections in a stage-n compound. When screening is strong, two of these sections are much larger than the remaining $n-2$ (for stage $n>2$). These two may be identified with boundary layer carriers, although, due to layer overlap (parameters γ_1,γ_4), a small percentage of the charge associated with these bands is actually on the interior layers. These large cylinders are insensitive to the small parameters γ_2,γ_5, and hence it is relatively easy to calculate their dispersion, even in the presence of intersandwich coupling, Γ_1.

The $n-2$ smaller cross sections are much more difficult to analyze, both for physical and mathematical reasons. Nevertheless, it is important to understand these areas, since they ultimately dominate the properties of very-high-stage compounds, transforming into the pockets of pure graphite. Hence subsection d involves a careful consideration of these smaller areas, with detailed equations for stages 3–6 included in Appendix A.

Some complications are purely mathematical—these bands are sensitive to the small parameters γ_2 and E_i, as well as to Γ_1, and by changing intercalants, Γ_1 can be varied from $\ll\gamma_2$ to $\gg\gamma_2$. A more serious problem, however, is that screening is imperfectly understood. Fermi surface studies[20] suggest that screening is incomplete in stage 3 and 4 acceptor compounds, with about 15% of the carriers residing on interior layers. However,

these studies are more sensitive to the boundary layers. Magnetoreflection studies[21] form a useful complement. These measurements of inter-Landau-level transitions are very sensitive to graphitic pockets, where both electrons and holes are present. Reflection oscillations are only observed in samples with $n \geq 4$, and for samples with $n \geq 6$ show bands very similar to pure graphite.

The detailed nature of screening will ultimately have to be worked out on the basis of experiment, and the equations in Appendix A are provided in a convenient form for use in data analysis. To gain a qualitative picture of the interior layers, however, the present manuscript makes a specific, simplifying assumption. It is assumed that the screening is nearly perfect: that all charge transferred into the graphite contributes to the large Fermi surface sections. In terms of Eq. (3), this means $E_{bF}=E_{F0}/2$ for $n \geq 2$. E_{i_F} is not, however, exactly zero, but is fixed by the conditions that the interior layers produce no net charge. In pure graphite, this leads to $E_{i_F} \cong \gamma_2$, with equal numbers of electrons and holes. Again, this model must be tested by comparison to experiment. It is likely that it will need modification in the transitional region, stages 3 and 4, but it should approach the correct result in the high-stage limit, and magnetoreflection[21] and other[19] studies suggest that it will be a useful approximation down to at least stage 5. For completeness, Appendix B very briefly discusses the solutions when screening is incomplete, and $E_i \neq 0$.

B. Special cases, $n = 1, 2, \infty$

For stages 1 and 2 there are no interior layers, and the results for the boundary layers have been derived previously,[7,8] and are included here for completeness. The dispersion relations are

$$|\Gamma_0|^2 = E_b(E_b - 2B\cos\phi) \quad (n=1)\,, \tag{4a}$$

$$[E_b^2-(\Gamma_0-\Gamma_4)^2][E_b^2-(\Gamma_0+\Gamma_4)^2]-4(B\cos\phi-\gamma_1) \times\Gamma_0\Gamma_4 E_b - E_b^2\,|\Gamma_1-\gamma_1|^2=0 \quad (n=2)\,, \tag{4b}$$

with approximate solution

$$|\Gamma_0| \cong |E_b| \mp B\cos\phi \quad (n=1)\,, \tag{5a}$$

$$|\Gamma_0| \cong |E_b| \pm(\gamma_1 - B\cos\phi)/2 \quad (n=2)\,, \tag{5b}$$

neglecting Γ_4 in stage 2. In stage 1, the $-(+)$ sign is for donors (acceptors), while in stage 2, there are two bands for either sign of carrier, associated with the $\pm$ sign. Note that the dispersion is approximately twice as large in stage 1, but E_b is also twice as large [Eq. (3)].

In the opposite, $n \to \infty$ limit (pure graphite), the boundary layers can be neglected, and Bloch's theorem used to collapse the $2n \times 2n$ determinant matrix into a 4×4, whose symmetric and antisymmetric parts are

$$[E_i \pm 2\gamma_1\cos\phi - 2\gamma_5\cos(2\phi)][E_i - 2\gamma_2\cos(2\phi)] - (\Gamma_0 \mp 2\Gamma_4\cos\phi)^2=0\,, \tag{6}$$

the well-known result for pure graphite. To understand the band structure of pure graphite, it is convenient to analyze the c-axis dispersion in the limit $k_\rho \cong 0$. This is illustrated in Fig. 1. There are four bands, two electronlike and two holelike. One pair is centered on $\pm 2\gamma_1\cos\phi$, the other (degenerate when $\Gamma_0=0$) about $2\gamma_2\cos2\phi$. Charge neutrality requires $E_F \cong 0$. In this case the γ_2 bands produce the electron and hole pockets of pure graphite, while the γ_1 bands may approximately be neglected.

C. $n \geq 3$: Approximation scheme and boundary layers

In what follows, the parameter γ_5 is neglected, B treated only to first order, and γ_2 treated only to "lowest order" (defined more precisely below). In this case, the determinant, Eq. (2), separates into symmetric and antisymmetric parts. If Γ_4 is written as $\Gamma_4 = \hat{\gamma}_4\Gamma_0$, where $\hat{\gamma}_4 = \gamma_4/\gamma_0 \cong 0.06$, the resulting determinant equations can be written as polynomials in Γ_0, of the following simple form:

$$(A_1\Gamma_0^2 + A_2)\Gamma_0^{m-2} + f = 0\,, \tag{7}$$

where m is the order of the determinant and f is a polynomial in Γ_0 of order Γ_0^{m-4}, which vanishes as $\gamma_2 \to 0$ (assuming E_i is of order γ_2). Hence, to sufficient accuracy, the boundary layer dispersion can be found by neglecting γ_2, as

$$A_1\Gamma_0^2 + A_2 = 0\,. \tag{8}$$

Moreover, for the interior layers Γ_0 is small, $\Gamma_0^2 \ll A_2/A_1$, so for the interior layers

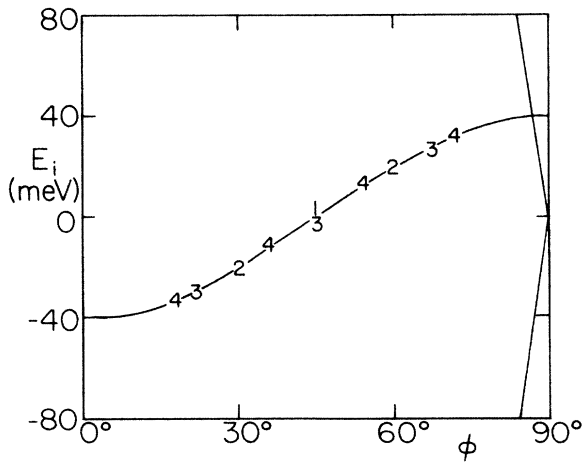

FIG. 1. c-axis dispersion for pure graphite (solid lines) at band bottom ($k_\rho=0$). In low-stage GIC's, this band breaks up into dispersionless cylinders (if B, B_2 are neglected). Numbers show position of bands (values of E_i) for various stages. As discussed in Appendix A, $N=1$ corresponds to stages 3–5, 2 to 5–7, 3 to 7–9, and 4 to 9–11.

$$A_2\Gamma_0^{m-2}+f=0\ . \tag{9}$$

Neglecting γ_1 and γ_4, the boundary layers have the same dispersion relation independent of stage:

$$|\Gamma_0| = |E_b| \mp B\cos(\phi/2),\quad n\geq 3\ , \tag{10}$$

just as in stage 2. More exact results, incorporating γ_1 and γ_4, are included in Appendix A and illustrated in Fig. 2. Equation (10) is true as long as $\gamma_4 > B$, but if $\gamma_4 \to 0$, the dispersion would fall off as $\hat{\gamma}_4^{n-3}$. This is because B couples the two boundary layers across an intercalant layer, whereas γ_4 is necessary to allow interlayer hopping within the sandwich.

D. $n \geq 3$: Interior layers

The solutions for interior layers are discussed in detail in Appendix A, with results shown in Figs. 1 and 3. The qualitative nature of these solutions may most easily be understood by ignoring coupling between sandwiches or with the bounding layers. Again, the analysis is simplified by first considering the $k_\rho = 0$ limit, just as for pure graphite. In this case Bloch's theorem may again be applied, and the solutions are *identical* to those of Eq. (6). However, now, to satisfy boundary conditions, ϕ is not a continuous variable but is limited to a few discrete values. As in pure graphite, these bands are associated with γ_1 or γ_2; since $\gamma_1 \gg \gamma_2 \cong E_i$, only the latter make a significant contribution to the Fermi surface, and only they will be considered in detail. For stage n, there are $n-2$ allowed values of ϕ, illustrated in Fig. 1. As n becomes large, these individual bands merge into the graphitic γ_2-band. For low n, however, each of these solutions provides a discrete, nearly cylindrical section of Fermi surface—the true dispersion comes from the parameters Γ_1 and Γ_2 and, in the case of acceptor compounds, may be much smaller than in pure graphite. Note, however, that magnetoreflection spectroscopy is predominantly sensitive to the in-plane Fermi surface parameters, and these will not differ greatly from pure graphite.

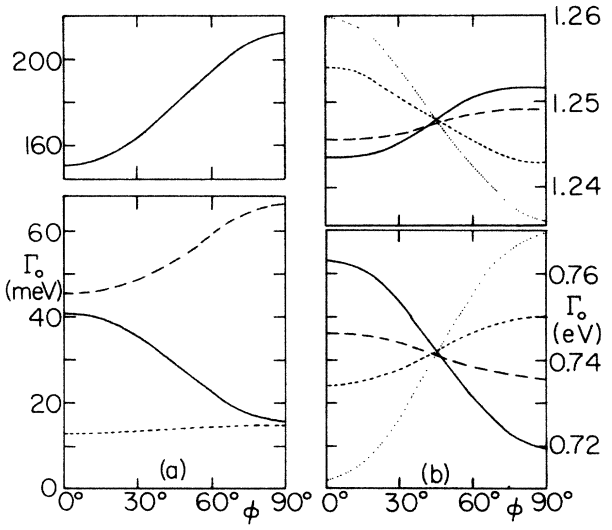

FIG. 2. Warping of the cylindrical Fermi surfaces: constant energy surface, Γ_0 vs ϕ, for acceptor GIC's with $E_b = -1$ eV, $E_i = 0$. Recall that $|\Gamma_0| = (\sqrt{3}\gamma_0 a_0/2)k_\rho$, $\phi = I_c k_z$, so that, up to a multiplicative constant, these are curves of k_ρ (k_z), showing the warping of the Fermi surface away from a perfect 2D cylinder, k_ρ is a constant. (a) Interior layers; (b) boundary layers. Dispersion has been exaggerated by choosing $B = 0.5$ eV. Dotted line, stage 3; short dashed line, stage 4; long dashed line, stage 5; solid line, stage 6.

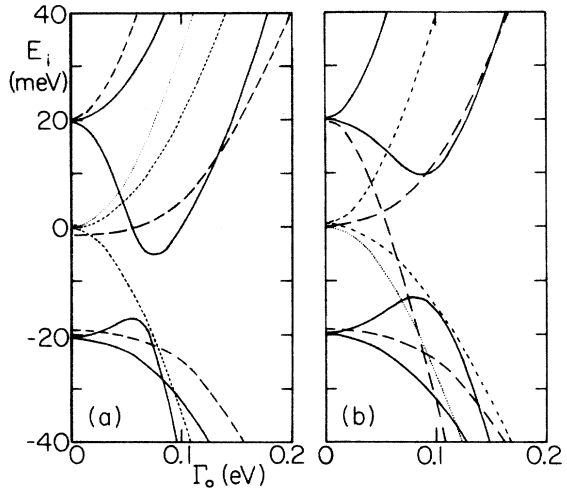

FIG. 3. Energy dispersion of graphitic bands in low-stage GIC's, with $\phi = 0$, $B = 2$ meV. Recall (caption of Fig. 2) that $\Gamma_0 \propto k_\rho$), so this is a standard dispersion relation, $E(k_\rho)$. Dotted line, stage 3; short dashed line, stage 4; long dashed line, stage 5; solid line, stage 6. (a) Acceptor compound ($E_b = -1$ eV); (b) donor compound ($E_b = 1$ eV).

The development of the graphiticlike interior bands can now be easily traced (Fig. 3). For stage 3, there is only one γ_2-like band and one γ_1-like band with a gap in between. Charge neutrality can be assured with E_i inside the gap (e.g., $E_i = 0$), so there are *no interior layer bands* expected for stage 3, unless screening is incomplete. For stage 4, there are two γ_2-like bands, one electronlike (for $k_\rho \neq 0$) and one holelike. At $k_\rho = 0$, these bands are degenerate, so the charge-neutral state is a zero-gap semiconductor. The overlap Γ_1 will not split the degeneracy, but a Γ_2-type overlap [see Eq. (2)] will provide a dispersion of the bands and hence produce electron and hole pockets similar to those in pure graphite (although with a different absolute value—and possibly sign—of dispersion). For higher n, new bands are added of alternate sign, so that for even n there are equal numbers of electronlike and holelike bands. For odd n, the extra band is holelike (electronlike) in an acceptor (donor) compound. For $n = 5$, there is band overlap for a donor compound, but not for acceptor compounds. For $n \geq 6$, there should be overlap for all stages, but there can be level-anticrossing effects, illustrated in Fig. 3 for stage 6.

In summary, it has been shown how the graphitic

bands develop in a GIC as the stage increases. There are no such bands in stages 1 and 2, and a single band in stage 3, which will probably be hard to observe, since the gap between it and the next band is fairly substantial. For stage $n \geq 4$, there is a series of bands which become more and more graphitic. There will be considerable difficulty in testing the detailed predictions of Fig. 3, however. For instance, magnetoreflection studies excite carriers from filled bands below the Fermi level to empty bands above it, and hence should look almost graphitic for $n \geq 4$. Careful study of the energy dependence could reveal that there is zero gap in stage 4. Transport studies, discussed below, will be dominated by the large boundary layer bands. Effects of the graphitic bands show up most prominently in the temperature dependence of the c-axis conductivity. However, this is mainly a population effect, as in semiconductors. In pure graphite, the degeneracy temperature is only 150 K and above this temperature the thermal excitation of carriers becomes significant. A very similar effect will occur in GIC's with a gap ≤ 150 K ($\sim\gamma_2$), as is true for all $n \geq 4$. Additional complications arise if imperfect screening shifts E_F from the charge-neutral position, or if the samples are imperfectly staged.

It should be stressed that, while the approximate calculations discussed here dealt only with the special case of neutral interior layers, the formulas in Appendix A are considerably more general; they can be used to treat both imperfect screening and inequivalent interior layers.

V. CONDUCTIVITY ANISOTROPY

A. Temperature dependence

The above calculations can be used either directly, in Fermi surface studies, or indirectly, in studies of the stage dependence of properties of GIC's. As an example of the latter, this section discusses the temperature and stage dependence of the conductivity anisotropy. The calculations for stage 1 (Ref. 7) can be generalized simply by using the appropriate dispersions and summing up over all bands. This model assumes that the scattering time τ is isotropic and the anisotropy is purely a band-structure effect. However, the stage dependence of the c-axis conductivity shows an unusual T dependence, varying from metallic (positive temperature coefficient of resistivity) in the low stages to activated (negative coefficient) in higher stages. To explain the effect requires inclusion of two additional effects: anisotropy in τ, and thermal excitation of interior layer carriers.

Since the conductivity involves a k-space average,[7] only a very strong anisotropy in τ will lead to a significant anisotropy in σ. For instance, if $\tau^{-1}=\tau_0^{-1}\sin^2\theta$ where τ_0 is a constant and θ is the tilt angle of the electronic k vector out of the conducting plane, the conductivity anisotropy changes by only a few percent from the value it would have for isotropic τ. Parenthetically, this justifies the assumption of Ref. 1 that the principal reason for anisotropy is due to band-structure effects. To introduce a very large anisotropy into τ, assume a process which produces no scattering in plane but strong scattering for $\theta > \theta_c$. A simple model of this is $\tau_{(\theta)}^{-1}=\tau_\perp^{-1}$ if $\theta > \theta_c$, $\tau^{-1}=\tau_\parallel^{-1}$ if $\theta < \theta_c$, where $\tau_\perp$ is the highly anisotropic scattering time, and $\tau_\parallel$ is due to all other sources. Note that $\tau_\parallel$ may be isotropic, but if $\tau_\parallel^{-1} \ll \tau_\perp^{-1}$, it can be ignored if $\theta > \theta_c$. Then it can be shown that to good approximation

$$\begin{aligned} \sigma_c \mid_{\text{anisotropic}} &\cong \sigma_c \mid_{\text{isotropic}} , \\ \sigma_a \mid_{\text{anisotropic}} &\cong \sigma_a \mid_{\text{isotropic}} \left[1+\frac{\tau_\parallel}{\tau_\perp}\theta_c\right] , \end{aligned} \tag{11}$$

where the isotropic values of σ are calculated with $\tau=\tau_\perp$. Even for a large anisotropy in τ, this mechanism leads to a small absolute change in the σ anisotropy, but can make a large change in the T dependence of that anisotropy. Since in GIC's the strongly anisotropic term is probably due to scattering by stacking faults,[22] $\tau_\perp$ can be taken as T independent.

Let us first apply this model to pure graphite. Band-structure effects (anisotropic effective masses) by themselves produce an anisotropy if $\sigma_a/\sigma_c \cong 100$, which is approximately the anisotropy observed in natural flake graphites. In highly oriented pyrolitic graphite (HOPG), $\sigma_a/\sigma_c \sim 1000$, suggesting $\theta_c\tau_\parallel/\tau_\perp \cong 10$. The model then predicts a metallic T dependence of σ_a, and σ_c approximately T independent. In fact it is found that σ_c increases as T increases. This can readily be understood. The Fermi surfaces are so small that the degeneracy temperature is only ~ 150 K, so the density is a function of T. The increase of n will cause a corresponding increase in σ_c, but only small effects compared to the intrinsic T dependence in σ_a. Since the interior layers of GIC's have comparable or smaller Fermi surfaces, the same effect should be observed there. On the other hand, the degeneracy temperature of the boundary layers is much higher, so for these layers n is constant and the only T dependence comes from $\tau_\parallel$. This provides a natural explanation for the observed stage dependence of the T-dependent anisotropy.

B. Stage dependence

From the results of Sec. IV, it is straightforward to predict the stage dependence of the conductivity anisotropy. Reference 7 showed that, given an isotropic τ and a dispersion relation of the form

$$\Gamma_0 = E^* + B\cos\phi , \tag{12}$$

the conductivity can be written

$$\sigma_a = e^2\tau \mid E^* \mid /\pi\hbar^2 I_c , \tag{13}$$

$$\sigma_c/\sigma_a = (BI_c)^2/2\eta_0^2 , \tag{14}$$

where $\eta_0=(\sqrt{3/2})\gamma_0 a_0$. These formulas only hold for open Fermi surfaces, $\mid B/E^* \mid \leq 1$. This restriction is certainly valid for the boundary layers in GIC's, and in general is a reasonable approximation for the interior layers in the low-T limit.

The conductivities of each band can be found from Eqs. (13) and (14), and the net conductivity is the sum

over the bands. Note that conductivities are generally measured per unit volume, as in Eq. (13). It is more natural, however, to discuss the conductivity *per sandwich*, $\bar{\sigma}=\sigma I_c$. Comparing Eqs. (3), (10), and (17), it can be seen that the in-plane conductivity $\bar{\sigma}_a$ has a stage-independent contribution, $\bar{\sigma}_a \propto E_{F0}$, due to charge transfer. In addition there is an extra contribution due to compensating electron and hole pockets in high-stage compounds. This monotonic increase in $\bar{\sigma}_a$ with stage could lead to a peak in σ_a at a particular stage. Experimentally, a peak of σ_a is observed[23] near stage 5. This peak may be enhanced by a tendency for the charge transfer per intercalant to be larger in higher-state compounds. More detailed discussion of the stage dependence of σ_a may be found in the literature.[6,24]

In the ideal screening limit, the c-axis conductivity may be written as a sum of boundary and interior layer contributions:

$$\frac{\sigma_c}{\sigma_a}=\frac{I_c^2}{2\eta_0^2}(B_b^2+B_i^2)\ . \tag{15}$$

Summarizing the results of Sec. IV,

$$B_b=\begin{cases}B, & n=1\\ B/2, & n>1\ ,\end{cases} \tag{16}$$

while $B_i=0$ for $n\leq 4$ (at $T=0$); for $n\geq 5$ its value depends on the exact value of E_F, and can be calculated using the formulas of Appendix A, but will make only a small correction to σ_c. Much more important is the temperature dependence of σ_c, due to thermal excitation of carriers in the graphitic bands.

Hence $\bar{\sigma}_a$ should have nearly the same magnitude and temperature dependence for all stages (the principal change being the variation of charge transfer with n). For stages 1–3, $\bar{\sigma}_c$ should have the same T dependence as $\bar{\sigma}_a$ (or should have a T-independent additional term due to stacking faults), while for $n\geq 4$, there should be a graphiticlike contribution with a positive temperature coefficient of resistivity, due to thermal excitation of carriers, whose magnitude grows with increasing number of layers. Because of the small dispersion of the graphitic bands, the low-temperature conductivity for a high-stage compound can be lower than in pure graphite, causing a stronger temperature dependence of σ_c than in pure graphite. These results are in general agreement with experiment.[15,25] It is hoped that the calculations of this paper will stimulate additional tests of the model. Finally, a knowledge of the band contributions to the conductivity in GIC's will allow a much clearer assessment of the role of hopping conduction.[26]

VI. USING THESE CALCULATIONS

The purposes of this paper have been twofold. First, to show in a sufficiently simple model how the graphite bands evolve in a GIC; secondly, to provide detailed enough formulas to allow experimental tests of these calculations. A number of caveats must be made to anyone who hopes to apply these formulas. First, despite over a decade of intense activity in studying GIC's, many of the fundamental parameters—including even the charge transfer—are not well known. It is not clear, for instance, whether the γ parameters depend on stage or intercalant. Since the lattice parameters of the graphite layers change so little upon intercalation, it is reasonable to assume that such change is small, and my studies of acceptor GIC's have shown that all the data can be interpreted using graphitic γ values. However, it should be pointed out that there is still uncertainty about the best values of these parameters for pure graphite, so small deviations from an accepted value may be revealing more about pure graphite than about a particular GIC.

Once the γ's are known, there are still a considerable number of parameters. These include the total carrier density n_0 [or, equivalently, E_{F0} of Eq. (3)]; the coupling constants *across* the intercalant layer, represented by B; and the screening parameters E_b, E_i. My suggestion is to use the simplest set of assumptions to analyze the data and only when these prove inadequate to go to more complicated assumptions. There are known to be significant sample-to-sample variations in n_0 for acceptor GIC, so it is difficult to say whether the small stage-to-stage variations observed are real, and it is dangerous to use a literature value of n_0 for more than order-of-magnitude estimation. The best way is to determine n_0 via de Haas–van Alphen measurements—although these can be complicated by imperfect staging, superlattice effects, torque or magnetic instability, or even simply the nonsinusoidal line shape expected for the oscillations near the two-dimensional limit. In lieu of these, in a study of stage dependence of conductivity, it is reasonable to assume that n_0 will be approximately constant for a series of similarly prepared samples (although detailed analysis may show that this is not the case). The interlayer coupling constants for stage 1 are reasonably well represented by Eq. (1),[7] and a good first approximation is to assume that this is stage independent. The distribution of carriers between boundary and interior layers (the ratio E_i/E_b) is the major unknown in the study of higher-stage compounds. For stages greater than 4 a simple assumption of graphitic interior layers[19] suggests that $E_i\cong 0$, and the figures of this paper are based on that assumption, although more general formulas are provided. The data should be analyzed by first assuming $E_i=0$, but should there be poor agreement between experiment and theory, this assumption should be the first one to vary. It is likely that $E_i\neq 0$, especially for stages 3 and 4, and it is hoped that future experiments will settle this question.

With the above points in mind, the present theory should be applicable to both donor and acceptor compounds. The only serious restriction occurs in some stage-1 donor compounds (K, Li) where there may be additional energy bands contributed by the donor atoms. This complication is particularly serious if the bands hybridize, so that none of the Fermi surface sections resemble those of the present calculation. However, the presence of these extra Fermi surfaces is by no means certain, and it is hoped that the present calculations (or those of Ref. 7) will be useful for these materials as well—by allowing concrete calculations for the case where the extra surfaces are absent. For instance, the small conductivity

anisotropy of these compounds can be understood without introducing new Fermi surfaces—since I_c is small for these compounds, c-axis overlap, and hence σ_c, are intrinsically large.

For the most quantitative applications, a further restriction should be noted. This applies only to the largest Fermi surface sections, and hence again primarily to low-stage donor compounds. The Slonczewski-Weiss-McClure model is only valid within about 1 eV of the K point. Beyond this point the band parameters no longer accurately represent the curvature of the energy bands, so estimates of carrier concentration are likely to be in error. An improved estimate can be made using the extended model due to Johnson and Dresselhaus.[17]

APPENDIX A: APPROXIMATE FORMULAS

The following results can be used for more detailed solutions of Eqs. (8) and (9) for intermediate-stage GIC.

1. Boundary layers

Writing $\bar{B}=B\cos\phi$, $E_{\pm}=E_b\pm\bar{B}$, the solutions of Eq. (8) are

$$\Gamma_0^2=\begin{cases}E_b(E_-+4\hat{\gamma}_4\gamma_1)/(1-2\hat{\gamma}_4^2)^2, & n=3,\ \text{symmetric}\\ E_bE_+, & n=3,\ \text{antisymmetric}\end{cases},$$

$$\Gamma_0^2=E_b[(E_{\mp})(1\pm\hat{\gamma}_4)^2-\hat{\gamma}_4\gamma_1(2\pm\hat{\gamma}_4)]/(1\pm\hat{\gamma}_4-\hat{\gamma}_4^2)^2,\quad n=4,$$

$$\Gamma_0^2=\begin{cases}E_b[(E_-)(1-2\hat{\gamma}_4^2)-2\hat{\gamma}_4\gamma_1]/(1-3\hat{\gamma}_4^2)^2, & n=5,\ \text{symmetric}\\ E_b[E_+-2\gamma_1\hat{\gamma}_4]/(1-\hat{\gamma}_4^2)^2, & n=5,\ \text{antisymmetric}\end{cases},$$

$$\Gamma_0^2=E_b\{(E_{\mp})(1\pm\hat{\gamma}_4-\hat{\gamma}_4^2)^2-\hat{\gamma}_4\gamma_1[2(1\pm\hat{\gamma}_4)^2\mp\hat{\gamma}_4^3]\}/[(1\pm\hat{\gamma}_4)(1-\hat{\gamma}_4^2)-\hat{\gamma}_4^2]^2,\quad n=6.$$

2. Interior layers: General results

Before solving Eq. (9) for particular stages, a brief discussion is given of the general case, sketching the proof of some general results quoted in Sec. IV D. While the discussion is valid for arbitrary stage, for illustrative purposes some results will be quoted for stage 6. After symmetrizing the wave functions the determinant becomes a product of two smaller (symmetric and antisymmetric) determinants. When $k_\rho=0$ (i.e., $\Gamma_0,\Gamma_4=0$), the stage-6 determinants become

$$\det\begin{bmatrix}-E_F & 0 & -\gamma_1 & 0 & 0 & 0\\ 0 & -E_b & 0 & 0 & 0 & \gamma_2\\ -\gamma_1 & 0 & -E_i & 0 & -\gamma_1 & 0\\ 0 & 0 & 0 & -E_i & 0 & \pm\gamma_2\\ 0 & 0 & -\gamma_1 & 0 & -\bar{E}_i\mp\gamma_1 & 0\\ 0 & \gamma_2 & 0 & \pm\gamma_2 & 0 & -\bar{E}_i\end{bmatrix}=0,$$

where the upper (lower) sign goes with the symmetric (antisymmetric) determinant, and $\bar{E}_i\neq E_i$ allows for different charging of the inequivalent interior layers. The odd rows (involving γ_1) and the even rows (involving γ_2) are now completely decoupled, so each determinant can be split into two 3×3's. The bands of interest, those associated with γ_2, are

$$\det\begin{bmatrix}-E_b & 0 & \gamma_2\\ 0 & -E_i & \pm\gamma_2\\ \gamma_2 & \pm\gamma_2 & -\bar{E}_i\end{bmatrix}=0.$$

Note the c-axis dispersion (associated with $E_{\pm}$) has completely gone. However, if there had been a term equivalent to Γ_2 in Eq. (2), the E_b would be replaced by $E_b\mp B_2\cos\phi$, restoring a dispersion. Ignoring this dispersion and noting $E_b\gg\gamma_2$, the boundary layers can be approximately decoupled, leaving

$$\det\begin{bmatrix}-E_i & \pm\gamma_2\\ \pm\gamma_2 & -\bar{E}_i\end{bmatrix}=0,$$

with solution (when $E_i=\bar{E}_i$) $E_i=\pm\gamma_2$.

For arbitrary stage, it is more convenient *not* to symmetrize the wave functions, but to immediately separate γ_1 and γ_2 terms. Ignoring boundary layers and setting all E_i's equal, the determinant matrix has the form

$$\det\begin{bmatrix}-E_i & 0 & \gamma_2 & 0 & \cdots\\ 0 & -E_i & 0 & \gamma_2 & \cdots\\ \gamma_2 & 0 & \cdots & & \end{bmatrix}=0.$$

Again odd and even rows decouple (this corresponds to B versus B' carbon atoms, just as the γ_1 terms are associated with the A atoms), leaving two determinants of tridiagonal form:

$$\det\begin{bmatrix}-E_i & \gamma_2 & 0 & \cdots\\ \gamma_2 & -E_i & \gamma_2 & \cdots\\ \vdots & \vdots & & \end{bmatrix}=0.$$

This equation has a solution of Bloch form, with wave functions $\psi_m\sim\psi_1 e^{i2m\phi}$. This yields the same solution as for pure graphite:

$$E_i=2\gamma_2\cos(2\phi),$$

but the first and last equation can only be satisfied if ϕ is a multiple of ϕ_N, where

$\phi_N = 90°/(N+1)$,

for an $N \times N$ matrix—recall that this can correspond to stage $2N+1$, $2N+2$, or $2N+3$. These solutions are illustrated for low stages in Fig. 1.

3. Interior layers: Stages 3–6

In writing Eq. (9), explicitly, only the lowest-order terms in γ_2 and E_i are retained in the coefficient of each power of Γ_0^2. The resulting equations are discussed by stage.

(a) *Stage 3.* The interior layer equation (symmetric only) is

$$\Gamma_0^2(E_- - 4\hat{\gamma}_4\gamma_1) = E_i(E_i E_- - 2\gamma_1^2) .$$

For $\Gamma_0^2 = 0$, the roots are $E_i = 0$, $2\gamma_1^2/E_-$. For arbitrary Γ_0, the smaller solution is illustrated for an acceptor GIC in Fig. 3(a), for a donor in Fig. 3(b). There is a gap between the two solutions with no charge carriers. The neutrality condition can only be maintained for E_i within this gap, so there are no carrier pockets in stage 3. [Note: Due to overlap of carriers from the boundary layer, there will be a net charging of the interior layer, unless E_i is suitably adjusted. The same is true for higher-stage compounds. In keeping with the approximation discussed in Sec. IV(a), this complication will be ignored.]

(b) *Stage 4.* Define $\hat{E}_b = (E_\mp)(1 \pm \hat{\gamma}_4)^2 - \gamma_1\hat{\gamma}_4(2 \pm \hat{\gamma}_4)$. Then, for symmetric and antisymmetric determinants (upper sign goes with symmetric),

$$\Gamma_0^2 E_b \hat{E}_b = (E_b E_i - \gamma_2^2)[(E_\mp)(E_i \pm \gamma_1) - \gamma_1^2] ,$$

with $\Gamma_0 = 0$ solutions: $E_i = \gamma_2^2/E_b$, $E_i = \mp\gamma_1 + \gamma_1^2/E_\mp$. Note that there are four solutions, one doubly degenerate. From the dispersions introduced when $\gamma_0 \neq 0$ it can be seen (Fig. 3) that the condition for charge neutrality is $E_i = \gamma_2^2/E_b$, and there are again no interior layer bands. Unlike the stage-3 case however, there is no longer an energy gap between electronlike and holelike bands—the system is a zero-gap semiconductor, and any deviation from the charge-neutrality condition will result in an interior layer band. Incorporating a Γ_2 term in Eq. (2) would lead to replacing $E_b \rightarrow E_b \mp B_2\cos\phi$, producing a genuine band overlap. Even without such deviations, at finite temperatures there will be thermally excited carriers in the two bands.

(c) *Stage 5.* The antisymmetric solution is

$$\Gamma_0^2(E_+ - 2\gamma_1\hat{\gamma}_4) = (E_i + \gamma_2)(E_i E_+ - \gamma_1^2) .$$

The symmetric equation is

$$\begin{aligned}
&\Gamma_0^4[E_-(1-2\hat{\gamma}_4^2)^2 - 2\hat{\gamma}_4\gamma_1] + \Gamma_0^2\gamma_1[\gamma_2(E_i - \gamma_2) + 4\hat{\gamma}_4 E_-(E_i + \bar{E}_i - \gamma_2)] \\
&\quad = (E_i - \gamma_2)(\bar{E}_i - 2\gamma_2^2/E_b)[2\gamma_1^2(2E_- + \bar{E}_i) - E_- E_i \bar{E}_i] \\
&\quad \cong 4\gamma_1^2 E_-(E_i - \gamma_2)(\bar{E}_i - 2\gamma_2^2/E_b) .
\end{aligned}$$

The approximate form assumes $E_i, \bar{E}_i \ll E_-, \gamma_1$. Here and in stage 6, a distinction is made between the two inequivalent interior layers, with E_i representing the outer layers, $\bar{E}_i$ the inner. In the analysis, the distinction will be ignored, and it will be assumed that $E_i = \bar{E}_i$. These solutions are plotted in Fig. 3, and reveal a small gap for acceptor compounds, but overlapping bands for donors. The Fermi level (E_i) will be adjusted in this case to produce equal numbers of electrons and holes.

(d) *Stage 6.* The symmetric and antisymmetric equations are (upper sign symmetric)

$$\begin{aligned}
&\Gamma_0^4\{E_\mp(1 \pm \hat{\gamma}_4 - \hat{\gamma}_4^2)^2 - \hat{\gamma}_4\gamma_1[2(1 \pm \hat{\gamma}_4)^2 \mp \hat{\gamma}_4^3]\} + \Gamma_0^2\gamma_1\{(\gamma_1 \pm E_\mp)\hat{\gamma}_4[\hat{\gamma}_4(E_i + 2\gamma_2) \pm 2(E_i + \bar{E}_i)] \pm E_\mp(2\gamma_2 - \bar{E}_i) + E_i\gamma_1\} \\
&\quad = -[E_i\bar{E}_i - \gamma_2^2(1 + E_i/E_b)][(\bar{E}_i \pm \gamma_1)(E_i E_\mp - \gamma_1^2) - \gamma_1^2 E_\mp] \\
&\quad \cong \gamma_1^2(E_\mp \pm \gamma_1)[E_i\bar{E}_i - \gamma_2^2(1 + E_i/E_b)] .
\end{aligned}$$

As can be seen in Fig. 3, there are well defined electron and hole pockets, with a real c-axis dispersion, due to level repulsion effects.

APPENDIX B: AWAY FROM PERFECT SCREENING

The previous discussion has dealt exclusively with the perfect screening limit, where the interior layer bands are charge neutral. This appendix briefly discusses the more general case when $E_i \neq 0$. In this case γ_2 can safely be ignored, and if γ_4 is also neglected, the determinant equation can easily be found for arbitrary stages:

$$D_n + 2B\cos\phi X_n = 0 \quad (n \geq 3) , \tag{B1}$$

where $X_3 = E_b C_b$, $X_n = -\gamma_1 E_i X_{n-1}$, $C_b = \gamma_1^2 E_i E_b$, $C = \gamma_1^2 E_i^2$, and D_n is found by recursion:

$$D_n = WD_{n-1} - CD_{n-2} , \tag{B2}$$

with $D_3 = W_b(W_i W_b - 2C_b)$, $D_4 = (W_i W_b - C_b)^2 - W_b^2 C$, and $W_{i(b)} = E_{i(b)}^2 - \Gamma_0^2$. As discussed in Sec. III, this result can be separated into symmetric and antisymmetric components. For instance, for stage 3,

$$W_b + E_b\bar{B} = 0, \quad \text{antisymmetric} ,$$

$$W(W_b - E_b\bar{B}) - 2\gamma_1^2 E_i E_b = 0, \quad \text{symmetric} .$$

The Fermi surfaces of stages 3 and 4 are discussed in greater detail in Ref. 19.

[1]E.g., T. Ando, A. B. Fowler, and F. Stern, Rev. Mod. Phys. **54**, 437 (1982); and the proceedings of the International Conferences on the Electronic Properties of Two-Dimensional Systems, most recently in Surf. Sci. **120** (1986).

[2]H. L. Störmer, J. P. Eisenstein, A. C. Gossard, W. Wiegmann, and K. Baldwin, Phys. Rev. Lett. **56**, 85 (1985).

[3]K. von Klitzing, G. Dorda, and M. Pepper, Phys. Rev. Lett. **45**, 494 (1980).

[4]These have been measured, usually by going to multilayer systems. See E. Gornik, R. Lassnig, G. Strasser, H. L. Störmer, A. C. Gossard, and W. Wiegmann, Phys. Rev. Lett. **54**, 1820 (1985), and J. P. Eisenstein, H. L. Störmer, V. Narayanamurti, A. Y. Cho, A. C. Gossard, and C. W. Tu, *ibid.* **55**, 875 (1985).

[5]M. J. Naughton, J. S. Brooks, L. Y. Chaing, R. V. Chamberlin, and P. M. Chaikin, Phys. Rev. Lett. **55**, 969 (1985).

[6]M. S. Dresselhaus and G. Dresselhaus, Adv. Phys. **30**, 139 (1981).

[7]R. S. Markiewicz, Solid State Commun. **57**, 237 (1986).

[8]R. S. Markiewicz, M. Meskoob, and B. Maheswaran, Phys. Rev. B **36**, 7859 (1987).

[9]J. C. Slonczewski and P. R. Weiss, Phys. Rev. **109**, 272 (1958); J. W. McClure, *ibid.* **108**, 612 (1960).

[10]J. Blinowski, H. H. Nguyen, C. Rigaux, J. P. Vieren, R. LeToullec, G. Furdin, A. Herold, and J. Melin, J. Phys. (Paris) **41**, 47 (1980).

[11]R. S. Markiewicz, Solid State Commun. **44**, 791 (1982).

[12]N. A. W. Holzwarth, Phys. Rev. B **21**, 3665 (1980).

[13]S. Y. Leung and G. Dresselhaus, Phys. Rev. B **24**, 3490 (1981); M. Shayegan, G. Dresselhaus, and M. S. Dresselhaus, *ibid.* **25**, 4157 (1982).

[14]H. Zaleski, P. K. Ummat, and W. R. Datars, J. Phys. C **17**, 3167 (1984).

[15]E. McRae, J. F. Marêche, and A. Herold, in *Graphite Intercalation Compounds: Extended Abstracts,* edited by M. S. Dresselhaus, G. Dresselhaus, and S. A. Solin (MRS, Pittsburgh, 1986), p. 152.

[16]R. Clarke and C. Uher, Adv. Phys. **33**, 469 (1984).

[17]L. G. Johnson and G. Dresselhaus, Phys. Rev. B **7**, 2275 (1973).

[18]L. Pietronero and S. Strässler, Solid State Commun. **32**, 1337 (1979).

[19]M. S. Dresselhaus, G. Dresselhaus, and J. E. Fischer, Phys. Rev. B **15**, 3180 (1977).

[20]R. S. Markiewicz, Phys. Rev. B **28**, 6141 (1983).

[21]E. Mendez, T. C. Chieu, N. Kambe, and M. S. Dresselhaus, Solid State Commun. **33**, 837 (1980).

[22]S. Ono, J. Phys. Soc. Jpn. **40**, 498 (1976); T. Tsuzuku, Carbon **17**, 293 (1979).

[23]E. McRae, D. Billaud, J. F. Marêche, and A. Herold, Physica B **99**, 489 (1980).

[24]M. Dresselhaus and S. Y. Leung, in Extended Abstracts of the 14th Biennial Conference on Carbon (Penn State, 1979), p. 496 (unpublished); S.-J. Tanuma and Y. Yosida, in *Graphite Intercalation Compounds: Extended Abstracts,* Ref. 15, p. 10.

[25]R. Powers, A. K. Ibrahim, G. O. Zimmerman, and M. Tahar, Phys. Rev. B (to be published).

[26]K. Sugihara, Phys. Rev. B **29**, 5972 (1984).